LANGMUIR

pubs.acs.org/Langmuir Article

Structure and Thermodynamics of Linear, Ring, and Catenane Polymers in Solutions and at Liquid—Liquid Interfaces

Saeed Akbari Shandiz, Gary M. Leuty, Hao Guo, Abdol Hadi Mokarizadeh, Joao M. Maia, and Mesfin Tsige*



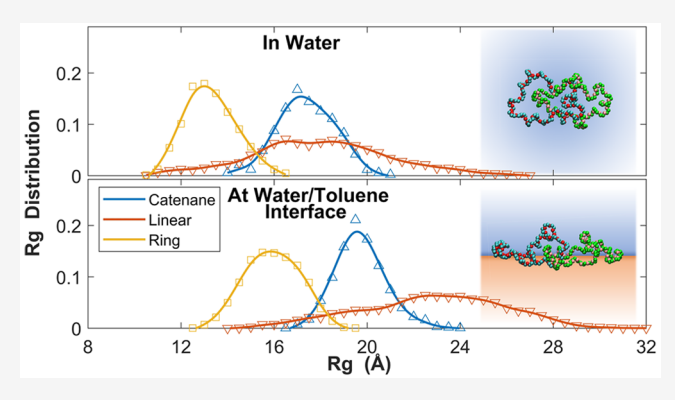
Cite This: Langmuir 2023, 39, 7154-7166



ACCESS

III Metrics & More

ABSTRACT: In recent decades, advances in the syntheses of mechanically interlocked macromolecules, such as catenanes, have led to much greater interest in the applications of these complexes, from molecular motors and actuators to nanoscale computational memory and nanoswitches. Much remains to be understood, however, regarding how catenated ring compounds behave as a result of the effects of different solvents as well as the effects of solvent/solvent interfaces. In this work, we have investigated, using molecular dynamics simulations, the effects of solvation of poly(ethylene oxide) chains of different topologies—linear, ring, and [2]catenane—in two solvents both considered favorable toward PEO (water, toluene) and at the water/toluene interface. Compared to ring and [2]catenane molecules, the linear PEO



Article Recommendations

chain showed the largest increase in size at the water/toluene interface compared to bulk water or bulk toluene. Perhaps surprisingly, observations indicate that the tendency of all three topologies to extend at the water/toluene interface may have more to do with screening the interaction between the two solvents than with optimizing specific solvent—polymer contacts.

INTRODUCTION

The behavior of macromolecules, especially polymers, in bulk solutions and at liquid/liquid interfaces is both scientifically and technologically important and has been the focus of much attention in recent years, given the various types of materials that can be successfully or even preferentially assembled in such environments. Polymers assemble in various ordered aggregates at liquid/liquid interfaces based on a number of factors, not the least of which are the individual interactions between the polymers and the solvents comprising the interface as well as the topologies of the polymers and how they array themselves at interfaces. The interplay between these factors is of paramount interest to researchers focused on the fabrication of novel two-dimensional materials exploiting liquid/liquid interfaces and the unique prospects they afford.

Liquid/liquid interfaces, as noted by Costa et al., ⁴ can serve as a "factory floor" for the self-assembly of two-dimensional nanostructures, and nanoparticles in particular, because "[nanoparticle]s are driven [to interfaces] by a reduction of interfacial energy." While the structure and dynamics of polymer topologies from linear to star^{5–7} and ring^{8,9} have been explored under many conditions (including in bulk solutions and at liquid/liquid interfaces^{7,10–13}) based on covalent bonding between monomers, comparatively little is known about the interfacial structure and dynamics of macro-

molecules that employ "topological bonds" in addition to chemical bonds, i.e., mechanically interlocked molecules.

In general, mechanically interlocked molecules are molecular assemblies in which two or more macromolecular components are entangled in such a way that while they are not chemically bonded to one another, the assembly as a whole cannot be separated without breaking chemical bonds between atoms within the separate components.¹⁴ The two archetypal categories of mechanically interlocked molecules are rotaxanes and catenanes. Rotaxanes consist of a macrocyclic component threaded by a linear macromolecule that features large or strongly interacting end groups (akin to a dumbbell) that prevent the macrocycle from unthreading. Catenanes, on the other hand, consist of two or more macrocycles threaded together akin to links in a chain (from which their name derives). 15,16 Catenation is a process that nature uses to control the conformations of molecular machines and supramolecular structures, two common examples being the

Received: March 3, 2023 Revised: April 27, 2023 Published: May 8, 2023





circular DNA catenanes^{15–22} and the "protein chain mail" that forms the capsid coats of bacteriophages^{23–25} and other viruses. Rotational freedom between rings makes catenanes promising as a class of components for molecular motors, ^{18,19} diagnostic equipment, ^{20,21} and rotors and actuators ^{22–25} as well as for molecular memory and nanoswitches. ^{26–28}

Initial attempts to synthesize catenanes relied on "statistical" threading, in which linear chains that pass through macrocycles in dilute solution are then cyclized to create a second closed loop in a chain. Further threading and cyclization could be performed to extend these chains, but statistical methods suffer from minuscule yields²⁹ due to the low probability of threading events in dilute or semidilute conditions (needed to enhance chain mobility) and the difficulty of maintaining a threaded state while performing the second (or third, or so on) cyclization. Subsequent years have seen the adoption of methods by which the interlocking of rings or ring precursor components could be maintained via covalent bonding between the components, followed by cleavage of the linking bonds to yield the final catenanes.³⁰ Decades later, chemists designed synthetic methods based on using reversible nonbonded interactions to hold components threaded in place (template-directed synthesis), substantially improving yields and allowing for more complex arrangements of catenanes. 26-28,31-36 These methods allowed for the synthesis and characterization of a wide array of catenanes at the level of individual macromolecular assemblies; however, characterizing the properties of catenane complexes and intra- and intercatenane interactions remains a challenge. As a result, little is known currently about the properties of catenanes, in general, and catenanes at interfaces, in particular.

Early computational investigations of [2]catenanes³⁷ and poly[n]catenanes³⁸ using lattice-based Monte Carlo simulations provided a preliminary understanding of the dynamical properties of bulk catenated polymers compared to their linear or ring counterparts. However, it was only after a years long pause, motivated by the more recent advances in synthesis,³ that the simulation community has returned to catenanes—for instance, de Pablo et al. ^{39–41} have more recently studied isolated poly[n] catenanes and the static and dynamic properties of melt poly[n] catenanes using molecular dynamics simulations. These studies centered on addressing fundamental questions concerning the melt properties of poly[n] catenanes, such as how the structure and dynamics of these polymers differ from their linear counterparts when the number of rings and the number of monomers per ring are systematically varied. The dynamics of poly[n] catenanes have been found to be slower than isolated linear polymers, which is believed to be a consequence of the entanglement effect resulting from the "mechanical bonds". 42 Furthermore, due to the excluded volume effect of the component rings in a catenated polymer, the repulsive forces between segments of a ring in a catenated polymer are stronger than in isolated ring polymers, and this in turn is expected to shift the θ -temperature of catenated polymers to smaller values compared to isolated ring polymers. 43 This effect is similar to the effect of topological excluded volume observed in star^{6,44} and ring^{45,46} polymers that results in a reduction of the θ -temperature compared to their linear counterparts.

While the findings from the previous studies are encouraging, there are still many unanswered questions about the physical properties of catenated polymers. The focus of the present work is the elucidation of structural and

dynamic differences between different polymer topologies compared to catenanes, and the effects imparted by different solvents, especially at interfaces between solvents. In particular, we seek to characterize catenanes that are currently accessible through known synthetic methods and are generally wellcharacterized, focusing on poly(ethylene oxide) (PEO) in linear, isolated ring and [2] catenane topologies in dilute solution, with water and toluene as solvents and at the water/ toluene interface. The ability of PEO to dissolve in organic (nonpolar) solvents such as toluene as well as water has led to the use of PEO as a model polymer for fundamental research as well as practical applications. The structure and dynamics of linear PEO polymers in aqueous solutions have been extensively investigated via simulation 47-52 and experiment, 52-57 and our results will be compared with the existing literature in order to elucidate the effect of catenation on the physical properties of polymers.

SIMULATION DETAILS

Linear, isolated ring and interlocked catenanes were constructed to investigate the effects of topology and catenation. For a linear PEO chain in water, the transition from ideal to real-chain behavior has been observed around a molecular weight $(M_{\rm w})$ of 2000. In this study, ring and linear PEO chains consist of 60 repeat units $(M_{\rm w} \approx 2640)$, much larger than the transition molecular weight. In the case of the [2] catenane, each of the PEO rings consists of 60 repeat units, so that the structure and dynamics of the rings in the [2] catenane can be directly compared with the other topologies. Chains of the three different polymer topologies were solvated in water (as a polar solvent), in toluene (as a nonpolar solvent), and at the water/toluene interface. Toluene and water are both considered to be good solvents for PEO but are mutually immiscible. Se

The three different PEO topologies were initially constructed with the help of Avogadro software. ⁵⁹ For samples in bulk solvent, [2] catenane PEO chains were placed inside a cubic box and solvated by adding sufficient numbers of water or toluene molecules to arrive at a dilute concentration of about 0.01 polymer weight fraction. The same numbers of water and toluene molecules were used for solvating the linear and ring PEO chains, resulting in concentrations of about 0.005 and 0.006 polymer weight fraction in water and toluene, respectively. The total number of atoms per simulation was around 90000 for PEO in water and around 75000 for PEO in toluene.

At the water/toluene interface, PEO chains were sandwiched between slabs of water and toluene in a rectangular simulation box. Though we expected the PEO to stay at the interface, we did not want to prevent PEO chain segments from segregating to either side of the interface should that occur, especially in the case of the catenane. To capture this possibility, the simulation box length in the direction normal to the interface was made much greater than the lateral dimensions (see below), necessitating many solvent molecules. The total number of atoms in simulations involving the water/toluene interface was therefore much larger, around 193000 (89373 water atoms, 102885 toluene atoms, and 840 PEO atoms).

All-atom molecular dynamics (MD) was chosen to provide the most accurate characterization of solvent effects, topology, and interface on the morphology and dynamics of solvated PEO chains. The Optimized Potentials for Liquid Simulations—All-Atom (OPLS-AA) force field was used for PEO

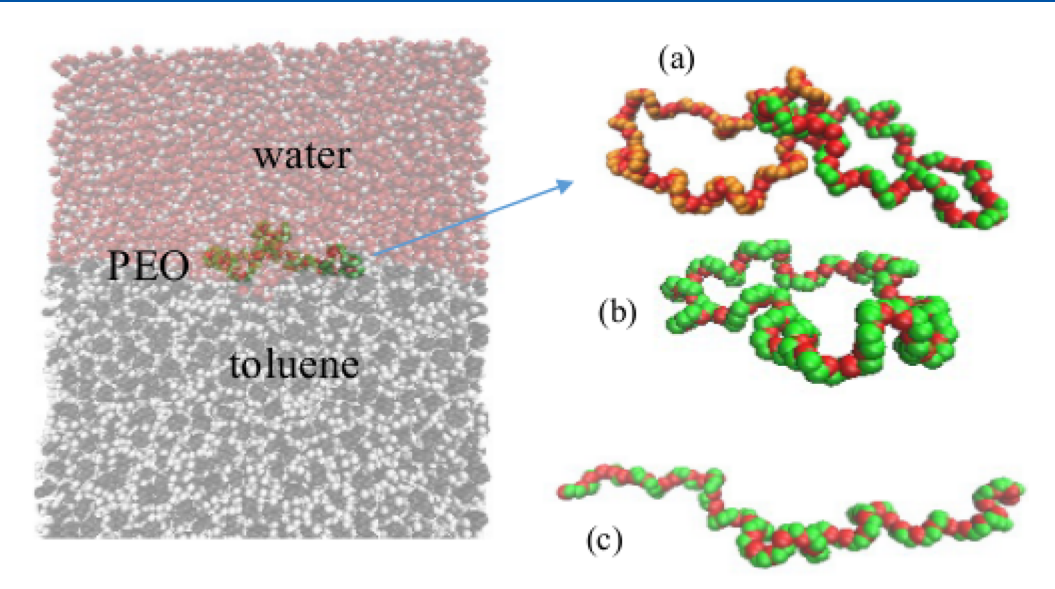


Figure 1. (a) PEO [2] catenane at the water/toluene interface. (b) An isolated view of the conformation of the [2] catenane at the interface (coloring scheme: O, red; C, green or orange; H, white) in order to show the conformations of the individual rings. (b) and (c) show the conformations of ring and linear polymer chains, respectively, at the interface. H atoms in (b) and (c) are not shown for clarity.

and toluene,⁶⁰ while the SPC/E model was employed for water. It has been shown that the original OPLS-AA partial charges for PEO are lower than needed to produce the correct structure of PEO in aqueous solution; thus, slightly modified charges⁵¹ were used in this study. Molecular dynamics simulations were conducted using the LAMMPS simulation package,⁶¹ with an integration time step of 1 fs and a Lennard-Jones cutoff radius of 12 Å in all simulations. The particle–particle/particle-mesh Ewald (PPPM) algorithm was used for the calculation of the Coulomb interactions.

Simulations were initially run in the NPT ensemble, with periodic boundary conditions in all directions, at a temperature of 300 K and at atmospheric pressure for 5 ns to allow the systems to reach their equilibrium density. The simulation box sizes after equilibration were approximately 96.5 Å \times 96.5 Å \times 96.5 Å for a PEO chain in bulk water or toluene and 103.7 Å \times 103.7 Å \times 199.8 Å for a PEO chain at the water/toluene system. Simulations continued in the NVT ensemble, with the duration of the run dependent on polymer topology. A simulation run of about 100 ns was deemed sufficient in the case of ring and catenane PEO systems, while roughly 300 ns was required for linear PEO systems. All water/toluene interface simulations were run for more than 300 ns, however, to ensure enough statistics for $R_{\rm g}$ distribution. Position data were recorded every 2 and 10 ps for PEO chains in bulk solvent and at the water/toluene interface, respectively, though postsimulation analysis of the data showed that a reporting frequency of 10 ps would actually have been sufficient for most of the structural and dynamic analysis. For hydrogen-bond calculations, including the hydrogen-bond autocorrelation function, simulations were extended for 1 ns, with position data recorded every 100 fs to capture initial fast and intermediate decay, and for 6 ns with data recorded every 2 ps to capture long-term decay.

■ RESULTS AND DISCUSSION

Chain Conformations at the Water/Toluene Interface. The PEO chains at the water/toluene interface generally exhibited a "pancake" structure similar to what is usually

observed for polymers adsorbed at solid/liquid interfaces. 62,63 However, the conformations of the rings of the [2] catenane around the catenation site deviated significantly from the pancake structure and were found to extend more toward the aqueous side of the interface (see Figure 1a). As a result, the interface in the region of the catenation site was perturbed, as can be observed from the figure. In general, the chains at the interface expanded markedly within the interface, with the linear chain extending into a rod-like conformation. Examination of the density profiles may be able to tell us if the perturbation of the interface around the catenation site had any major effects on the interfacial width compared to the ring and linear cases.

The mass density profiles of water, toluene, and PEO across the interface are shown in Figure 2. The computed averaged bulk densities of water and toluene away from the interface are

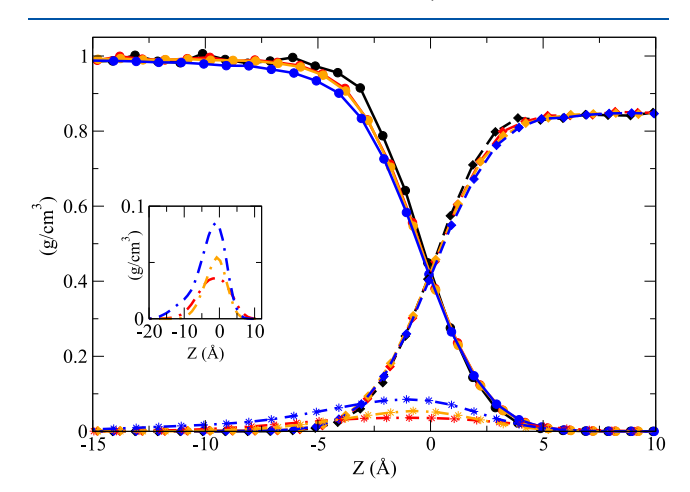


Figure 2. Mass density profiles of water (filled circles), toluene (filled diamonds), and PEO (inset or stars) close to the water/toluene interface in simulations of linear PEO chains (red), ring PEO chains (orange), and [2] catenane chains (blue). The densities of water and toluene in the absence of PEO are also shown in black for comparison.

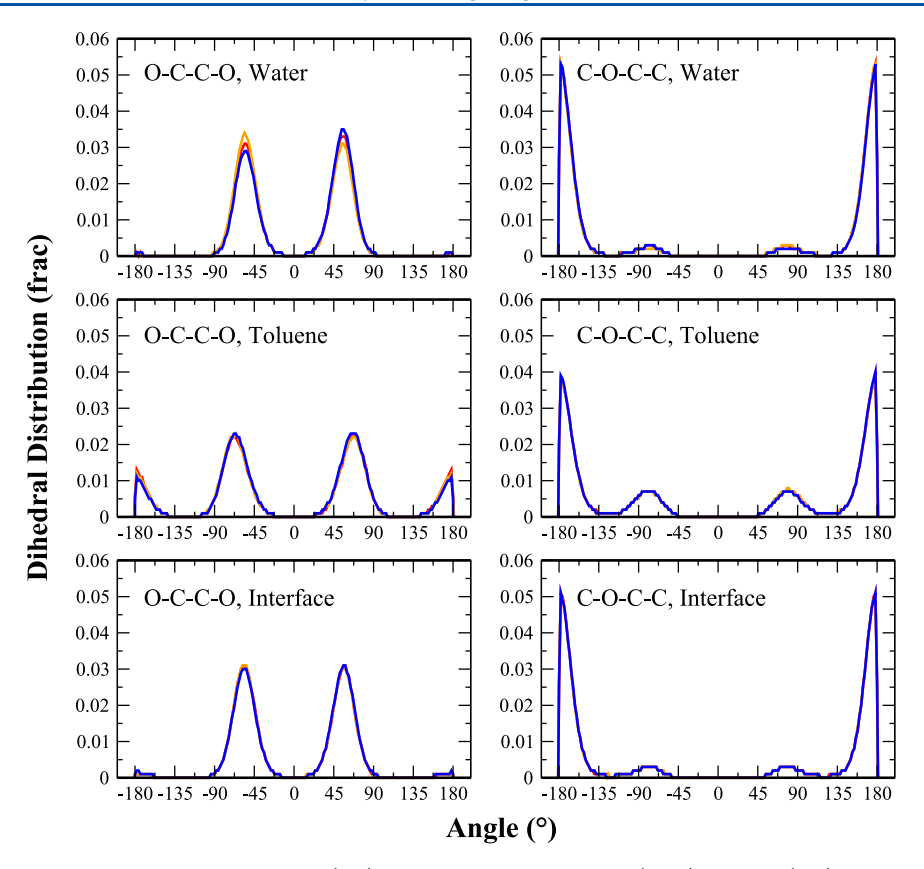


Figure 3. Dihedral distributions of O-C-C-O dihedrals (left) and C-O-C-C dihedrals (right) in water (top), in toluene (middle), and at the water/toluene interface (bottom) for linear PEO (red), ring PEO (orange), and [2]catenane PEO (blue).

 0.994 ± 0.001 and 0.847 ± 0.001 g/cm³, respectively, in very good agreement with reported experimental values.⁶⁴ In all cases, the middle of the interface is located around z=0. As a reference, water and toluene density profiles for the water/toluene system without a PEO chain are also included in the figure. Interestingly, the water—toluene interface does not show any dependence on chain topology and is only slightly perturbed in the presence of a PEO chain at the interface.

The density profiles of the different PEO topologies, shown in the inset of Figure 2, can be interpreted as the probability of finding a segment of a given PEO chain in the direction normal to the interface. These density profiles suggest that PEO chains are confined within the water/toluene interface at all times, with any extension away from the interface favoring water. The density profile of the [2] catenane PEO illustrates this extension into the aqueous side of the interface, as was alluded to in Figure 1a. Compared to the density profile of ring PEO, the density profile of linear PEO is slightly wider. However, the density of the single PEO chain at the interface is very small and does not affect the interfacial width.

Furthermore, from analysis of PEO conformations such as those seen in Figure 1, we observed that the PEO chains in general adopted helical conformations at the water/toluene interface, similar to what we have observed in bulk water (not shown) and what has been observed by experiments and simulation of PEO in aqueous solutions. The helical structure of PEO is characterized by a predominantly gauche conformation about the C–C bond and a predominantly trans conformation about the C–O bond, as shown in Figure 3. As expected for a helical conformation, the O–C–C–O and C–O–C–C distributions show an almost complete preference for

gauche conformations (>92%) in bulk water and a similar preference for trans conformations (>87%) at the water/toluene interface, independent of PEO topology, which is in excellent agreement with experimental results from NMR. 65,66

In toluene, however, there is a noticeable fraction of O-C-C-O dihedrals in the trans conformation (>22%) and a significant population of C-O-C-C dihedrals (>33%) in the gauche conformation, independent of PEO topology; as a result, we observe that the helical structure is lost. The adoption of these conformations results in a decrease of the total dihedral energy of the O-C-C-O and C-O-C-C dihedrals by about 7 and 8 kcal/mol, respectively, for linear and ring PEO chains in water and at the water/toluene interface compared to these same chains in toluene. The decrease is almost double in the [2] catenane case, which is proportional to the number of dihedrals in the [2] catenane chain. The observed decrease in the total dihedral energy can be explained through the conformational energy difference between the gauche and trans states of a given dihedral.

The gauche-trans conformational energy difference for O-C-C-O and C-O-C-C dihedral angles is about -0.6 and 0.26 kcal/mol, respectively, based on the OPLS force field. There are 59 O-C-C-O dihedrals and 118 C-O-C-C dihedrals in 60-mer PEO. Given that there are at least 18% more O-C-C-O dihedrals in the trans conformation (i.e., about 11 dihedrals) in toluene compared to water, this results in a total difference of more than 6 kcal/mol, which is comparable to the value reported above based on the torsional energy extracted from the simulation. Similarly, the excess 20% of C-O-C-C dihedrals in the gauche conformation in toluene compared to water results in a total difference of more

than 6 kcal/mol, which is also comparable to the value reported above.

The gauche conformations of the C-C bonds in PEO are expected to reduce the distance between PEO ether oxygens. Examination of the first peak location in the pair distribution functions between ether oxygens, shown in Figure 4, clearly

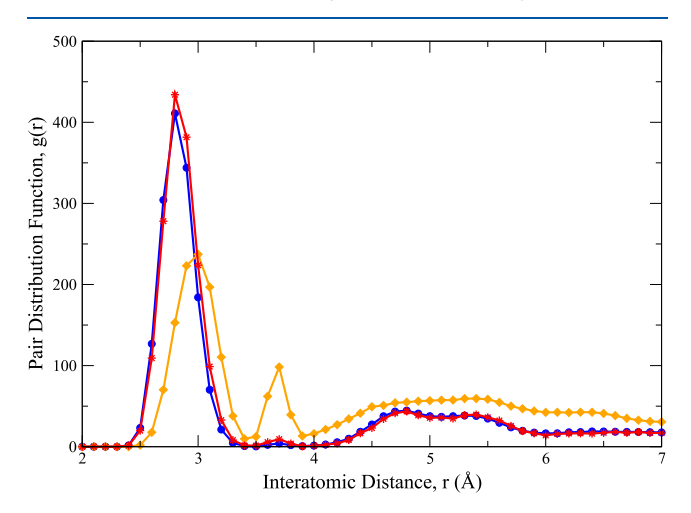


Figure 4. Pair distribution functions for PEO oxygen atoms in water (blue, filled circles), in toluene (orange, filled diamonds), and at the water/toluene interface (red, stars).

shows that the distance between the ether oxygens is reduced and nearly identical in water and at the water/toluene interface compared to its location in toluene, confirming our expectation.

Based on our observations so far, we can hypothesize that the conformations of PEO chains at the water/toluene interface must be dominated by interactions with the aqueous side of the interface because the dihedral distributions in bulk water and at the interface appear identical. This is discussed in further detail in the context of hydrogen bonding later in this work.

Molecular Dimensions. We first investigated the effects of polymer topology on the dimensions of PEO chains in bulk solution and at the water/toluene interface. The molecular dimensions of a polymer can be characterized by the radius of gyration, $R_{\rm g}$, a quantity also accessible through experiments. Ample amounts of experimental and simulation $R_{\rm g}$ data exist for linear PEO in aqueous solution that can be used for the validation of our simulation results. $^{50-52,55,68}$ We have used the following two expressions for calculating the time-averaged $R_{\rm g}$ of PEO polymer chains in bulk solvent and at the water/toluene interface:

$$R_{\alpha\beta}^{2} = \frac{1}{M} \langle \sum_{i=1}^{N} m_{i} (r_{\alpha}^{i} - r_{\alpha}^{\text{CM}}) (r_{\beta}^{i} - r_{\beta}^{\text{CM}}) \rangle$$
(1)

$$R_{\rm g}^{\ 2} = \frac{1}{M} \langle \sum_{i=1}^{N} m_i (r^i - r^{\rm CM})^2 \rangle$$
 (2)

where N is the total number of PEO atoms in a chain, m_i is the atomic mass of atom i, and M is the molecular weight of the chain. Equation 1 represents the elements of the radius of gyration tensor, ⁶⁹ where r^i_{α} and r^i_{β} represent the components of $\vec{r}^{(i)}$ of atom i in the three Cartesian directions $(\alpha, \beta \text{ run over } x, y, \text{ and } z)$ and CM denotes the center of mass of the chain. The

radius of gyration of the chain is then the sum of the eigenvalues of the tensor, $R_{\rm g}^2 = \lambda_1^2 + \lambda_2^2 + \lambda_3^2$. The eigenvalues— λ_1^2 , λ_2^2 , and λ_3^2 —will be helpful in determining the shape of the chain. Equation 2 represents the radius of gyration in a fixed rectangular coordinate system, where the components $R_{\rm g,z}^2$, $R_{\rm g,y}^2$, and $R_{\rm g,z}^2$ will be helpful in determining the perpendicular and parallel components of $R_{\rm g}^2$ at the water/toluene interface.

Figure 5 shows the time evolution of the radius of gyration of linear PEO chains in water, in toluene, and at the water/

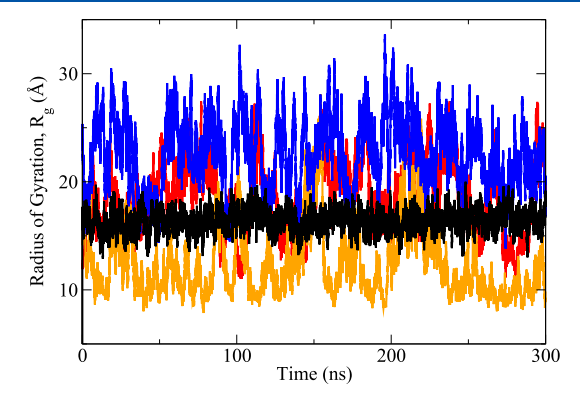


Figure 5. Radius of gyration as a function of time for linear PEO in water (red), in toluene (orange), and at the water/toluene interface (blue). For comparison, the $R_{\rm g}$ of ring at the water/toluene interface is also shown (black).

toluene interface. For comparison, the $R_{\rm g}$ of the ring chain at the water/toluene interface is also shown. While the $R_{\rm g}$ of the linear PEO chain displays significant oscillation as a function of time both in bulk solvent and at the water/toluene interface, the $R_{\rm g}$ of the ring is relatively stable both in bulk solvent and at the water/toluene interface (the [2]catenane shows similar behavior)—this justifies the relatively short simulation times (100 ns) for ring and [2]catenane molecules in water and toluene. The conformation of the linear chain oscillates between coiled (small $R_{\rm g}$) and extended (large $R_{\rm g}$). The dynamic conformational changes of the linear PEO chain, however, do not affect the interfacial width, as seen in Figure 2.

The R_g results for the different simulated cases can be summarized in the form of the radius of gyration distributions shown in Figure 6 and tabulated in Table 1. Both water and toluene are considered good solvents for PEO, but water is clearly the better solvent. For comparison, we ran an additional simulation of the linear PEO chain in a vacuum, expecting it to enter a globular conformation because PEO in a vacuum will interact favorably with itself and thus collapse. The linear PEO chain collapsed to a globule with $R_g = 7.7 \pm 0.2$ Å, which is about 40% smaller than the linear PEO chain in toluene. Note that the standard deviation of $R_{
m g}$ in the vacuum is very small, as would be expected for a polymer chain in a collapsed, globular conformation, while the standard deviation of the chain's R_{σ} in toluene is quite large, as would be expected for a polymer chain in an expanded coil conformation, due to large fluctuations in the conformation of the chain.

The $R_{\rm g}$ of linear, ring, and [2]catenane PEO in bulk water increased by about 50, 30, and 48%, respectively, compared to their $R_{\rm g}$ in bulk toluene. For linear PEO in water, a power law relation of $R_{\rm g}=0.20\times M_{\rm w}^{0.58}$ (Å) was reported from light scattering data from chains of large molecular weight. For linear 60-mer PEO, this relation gives an $R_{\rm g}$ value of 19.3 Å,

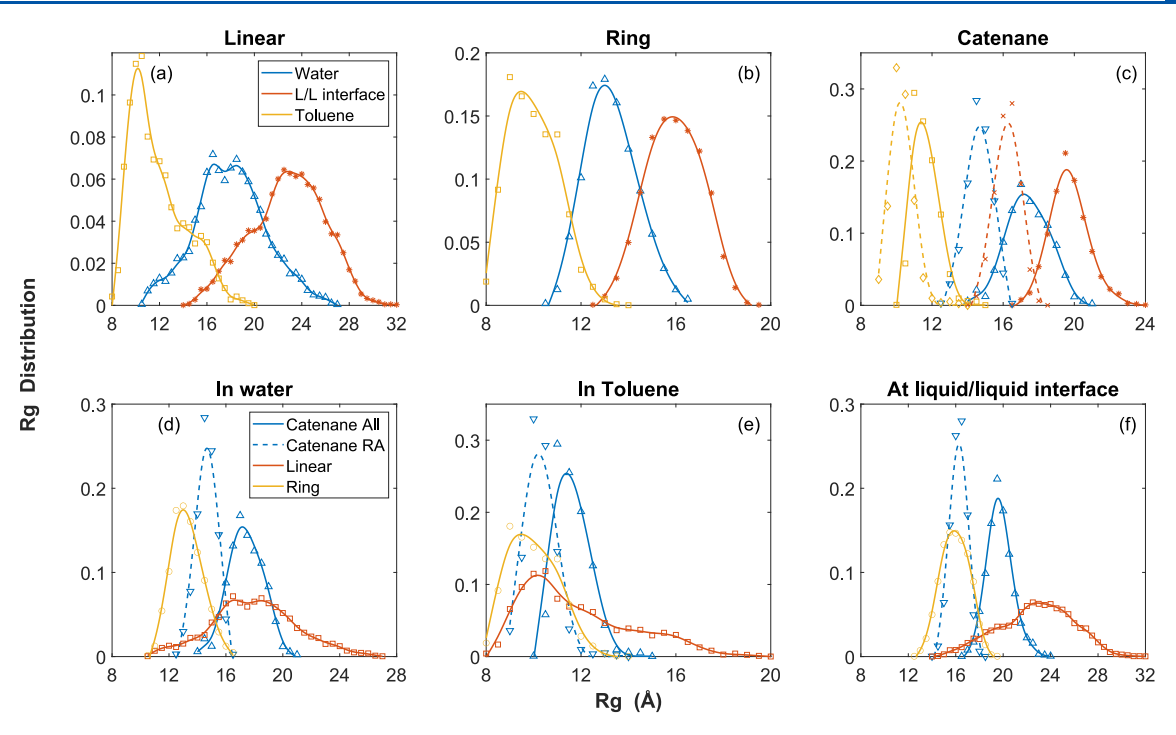


Figure 6. Radius of gyration (R_g) distributions of (a) linear, (b) ring, and (c) [2] catenane PEO chains in water (blue), in toluene (yellow), and at the water/toluene interface (red). The distributions of linear (yellow), ring (purple), and [2] catenane (blue, red) chains (d) in water, (e) in toluene, and (f) at the water/toluene interface are also shown. The broken curves represent the average ("RA": ring average) of the distributions of the two rings in the [2] catenane.

Table 1. Radius of Gyration $(R_g, Å)$ for Linear, Ring, and [2] Catenane PEO in the Different Solvents^a

PEO topology	water	toluene	W/T interface
linear	18.4 ± 3.0	12.3 ± 3.2	22.6 ± 3.2
ring	13.5 ± 1.1	10.4 ± 1.1	16.4 ± 1.0
[2]catenane			
whole	17.6 ± 1.2	11.9 ± 0.8	20.8 ± 1.7
ring avg	14.9 ± 0.7	10.5 ± 0.6	16.5 ± 0.7
larger ring	15.5 ± 0.9	11.2 ± 1.2	17.1 ± 0.8

"The [2] catenane case is split into the overall R_g , the ring-average R_g , and the ring with the larger R_g . Error bars were generated from time averaging over 100 ns.

which is in very good agreement with our simulation data for linear PEO in water at 18.4 \pm 3.0 Å (see Table 1). This $R_{\rm g}$ value is larger than that of linear PEO in toluene but smaller than that of linear PEO at the water/toluene interface. Furthermore, the $R_{\rm g}$ distributions show that a PEO chain, independent of topology, has a larger radius of gyration at the water/toluene interface than in either of the two bulk solvents (Figures 6a–c). The $R_{\rm g}$ of linear PEO at the water/toluene interface increased by about 23 and 84% compared to bulk water and toluene, respectively. Similarly, the $R_{\rm g}$ of the ring and [2] catenane at the water/toluene interface increased by about 22 and 18%, respectively, compared to their $R_{\rm g}$ s in bulk water and by about 50 and 74%, respectively, compared to their $R_{\rm g}$ s in bulk toluene. The $R_{\rm g}$ of the linear PEO chain, as expected, is larger than the corresponding $R_{\rm g}$ of the ring PEO chain.

Surprisingly, $R_{\rm g}$ for the linear PEO chain is larger than $R_{\rm g}$ for the whole [2] catenane, both in bulk solution and at the water/toluene interface, despite the fact that the degree of polymerization of the whole [2] catenane is twice that of the linear chain. This implies that the catenation of rings in

[2] catenanes does not necessarily produce an "extended-chain" catenane assembly: perhaps the rings of the catenane are more akin to slightly offset rings rather than a stretched chain. This suggests that the ratio of $R_{\rm g}$ for analogous [2] catenanes and linear polymers is $\langle R_{\rm g}^{\ 2} \rangle_{\rm catenane}/\langle R_{\rm g}^{\ 2} \rangle_{\rm linear} < 0.5$, which is even smaller than the ratio between ring and linear polymers, which in the current simulation is larger than 0.73. The reported literature values for the $\langle R_{\rm g}^{\ 2} \rangle$ ratio between ring and linear polymers is 0.52–0.6 from simulations of polystyrene under different solvent conditions and 0.56–0.73 from experiments involving polystyrene in θ -solvent. Our preliminary hypothesis based on our current result is $\langle R_{\rm g}^{\ 2} \rangle_{\rm catenane} < \langle R_{\rm g}^{\ 2} \rangle_{\rm ring} < \langle R_{\rm g}^{\ 2} \rangle_{\rm linear}$ in good solvent and at the liquid/liquid interface; we plan to confirm this as a function of chain length in future investigations using a bead—spring model.

The data for ring-average and larger-ring R_g in the [2]catenane case reported in Table 1 indicate that rings of [2]catenane PEO are more swollen than the corresponding free PEO ring in bulk solution and at the water/toluene interface; this is in agreement with recent results from lattice Monte Carlo simulation. However, our observation from careful examination of the R_g s of the two rings of the [2]catenane in water as a function of time is that most of the time both rings are more swollen than the corresponding free PEO ring in water, while in toluene, one of the rings is more swollen and the other ring is less swollen than the corresponding free PEO ring in toluene.

Furthermore, we can quantify information about the shape of the PEO chains in different conditions by extracting the eigenvalues of the radius of gyration tensor ($\lambda_1 < \lambda_2 < \lambda_3$). The quantities of asphericity (a) and prolateness (p) defined below are usually used for this purpose:⁷²

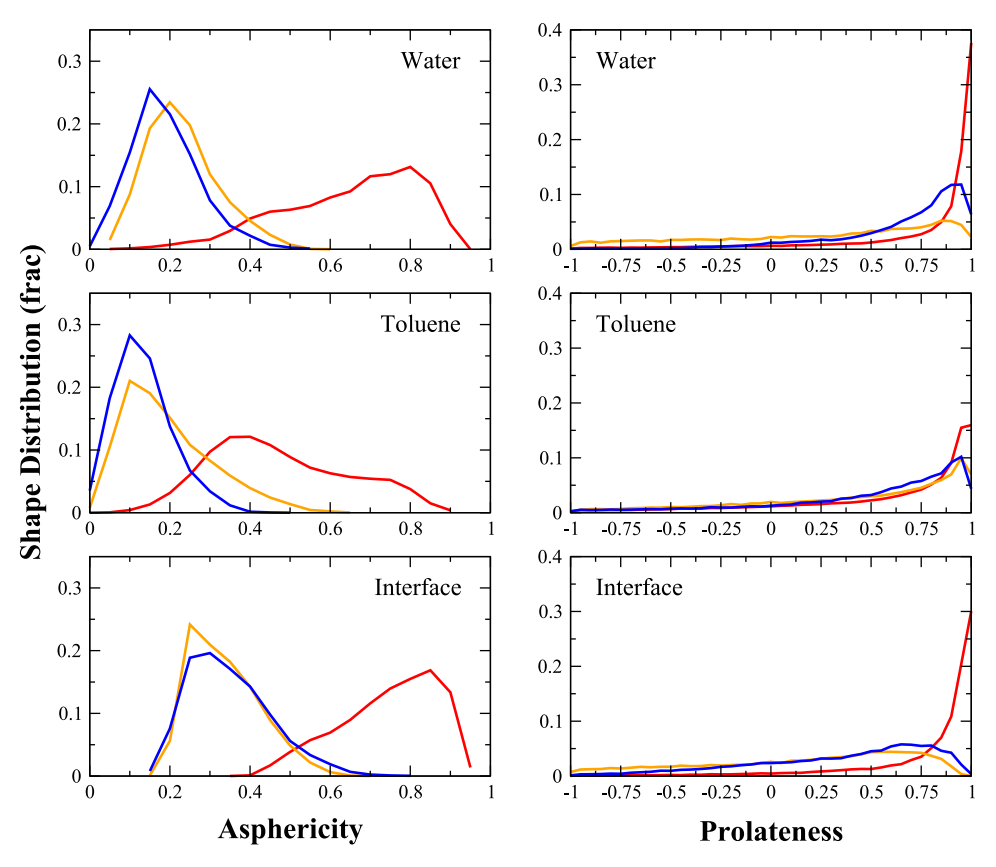


Figure 7. Probability distributions of the asphericity (left column) and prolateness (right column) for linear PEO (red), ring PEO (blue), and [2] catenane PEO (yellow) for polymer in water (top row), in toluene (middle row), and at the water—toluene interface (bottom row).

$$a = \frac{(\lambda_2 - \lambda_1)^2 + (\lambda_3 - \lambda_1)^2 + (\lambda_3 - \lambda_2)^2}{2(\lambda_1 + \lambda_2 + \lambda_3)^2}$$

$$p = \frac{(2\lambda_1 - \lambda_2 - \lambda_3)(2\lambda_2 - \lambda_3 - \lambda_1)(2\lambda_3 - \lambda_2 - \lambda_1)}{2(\lambda_1^2 + \lambda_2^2 + \lambda_3^2 - \lambda_1\lambda_2 - \lambda_2\lambda_3 - \lambda_1\lambda_3)^{3/2}}$$
(4)

For a perfectly spherical shape $(\lambda_1 = \lambda_2 = \lambda_3)$, both a and p are zero. Deviation from a perfect sphere results in $0 < a \le 1$, with a closer to 1 when the shape deviates significantly from a sphere (linear/planar). The range of values for prolateness is $-1 \le p \le 1$, where p = 1 represents a perfectly prolate shape $(\lambda_1 = \lambda_2 < \lambda_3)$, i.e., stretched in one principal direction, making the shape more rod-like) and p = -1 is a perfectly oblate shape $(\lambda_1 < \lambda_2 = \lambda_3)$, i.e., stretched in two principal directions, making the shape more "pancake"-like).

The distributions of asphericity and prolateness for all the cases are shown in Figure 7. The asphericity distributions show two distinct behaviors, with the distributions for linear PEO in water and at the water/toluene interface showing marked deviation from what would be expected of a sphere, more so even than the predicted asphericity of Gaussian linear chains. PEO linear chains in toluene also deviated notably from spherical, but not to the extent of chains in water and at the water/toluene interface, showing a hint of a bimodal distribution, with one mode less aspherical than a theoretical Gaussian linear chain and a smaller fraction significantly more aspherical. On the other hand, the asphericity distributions for ring and catenane PEO chains in water and toluene suggest a more spherical shape, deviating slightly when in bulk solvent (mean around 0.1–0.2) and noticeably more (mean around

0.3–0.4) for chains at the water/toluene interface. The asphericity distributions for linear PEO are generally asymmetric and largely left-skewed for linear PEO in water or at the water/toluene interface, while the distributions for ring and catenane PEO are much more symmetric (or partially right-skewed). A similar behavior can also be observed in the distribution of $R_{\rm g}$, shown in Figure 6, a result of the dynamic chain conformation observed for the linear PEO chain.

The prolateness distributions shown in Figure 7 (right column) indicate that chains of all topologies, but especially linear PEO in bulk water and at the water/toluene interface, exhibit highly prolate shapes. Surprisingly, the ring PEO in toluene and the catenane PEO in toluene and water show average shapes close to rod-like, which was not obvious from the asphericity distributions. Prolateness distributions for ring and catenane PEO at the water/toluene interface and ring PEO in water show a less starkly peaked distribution but remain predominantly prolate, with a large left-handed tail.

The end-to-end distance values for linear PEO in water, in toluene, and at the water—toluene interface were calculated to be 48.7 ± 16.2 , 17.4 ± 6.7 , and 62.2 ± 16.1 Å, respectively. Note that the end-to-end distance value for the linear polymer in water is in good agreement with recent experimental results. ⁵² Put together, the prolateness distribution and the end-to-end distance values indicate that the linear PEO chain at the water/toluene interface is primarily stretched in one direction (rod-like) while the same chain in toluene is in a slightly more collapsed state. The ring and catenane molecules, however, behave very similarly in terms of shape descriptors, suggesting that the shape of the catenane molecule in these environments is more affected by its component nature than

Table 2. Hydrogen-Bonding Statistics (Normalized by the Number of PEO Monomers) for Given PEO Topologies in Bulk Water or at the Water-Toluene Interface

	topology	⟨H-bonds⟩ ^a	$\langle H_2 O \rangle^b$	$single^c$	double ^c	triple ^c
H_2O	linear	1.47 ± 0.08	0.86 ± 0.05	0.40 ± 0.07	0.35 ± 0.05	0.11 ± 0.04
	ring	1.45 ± 0.08	0.83 ± 0.05	0.36 ± 0.07	0.35 ± 0.05	0.11 ± 0.04
	[2]catenane	1.48 ± 0.06	0.85 ± 0.03	0.37 ± 0.05	0.36 ± 0.04	0.12 ± 0.03
H_2O/Tol	linear	1.31 ± 0.08	0.75 ± 0.05	0.32 ± 0.06	0.33 ± 0.05	0.10 ± 0.04
	ring	1.31 ± 0.08	0.75 ± 0.05	0.31 ± 0.06	0.33 ± 0.05	0.11 ± 0.04
	[2]catenane	1.32 ± 0.06	0.75 ± 0.07	0.32 ± 0.05	0.33 ± 0.04	0.10 ± 0.03

[&]quot;Time-averaged number of hydrogen bonds between H₂O and PEO oxygens. "Time-averaged number of H₂O molecules involved in hydrogen bonding with PEO oxygens. "Contributions to (b) from water molecules making 1, 2, or 3 hydrogen bonds with PEO.

by the inclusion of the topological bond, which produces enlargement of the overall structure, but not necessarily a change in conformation.

Hydrogen Bonding. The results so far demonstrate that chain topology has an effect on the conformations of PEO chains in dilute solution. In the case of PEO chains in water and at the water/toluene interface, it is also important to investigate the correlation between chain conformation and hydrogen bonding with the surrounding water molecules. Hydrogen bonding is often characterized in terms of geometric definitions, such as distance-only or distance-angle cutoffs. For calculating hydrogen bonds, we used the distance-angle cutoff approach, with the distance cutoff for PEO oxygen—water hydrogen distance $r_{\rm OH} \leq 2.675~{\rm \AA}^{47}$ and the cutoff for PEO oxygen—water hydrogen—water hydrogen—water oxygen angle at $\theta_{\rm OHO} \geq 120^{\circ}.^{73}$

The hydrogen-bond calculation results are summarized in Table 2. Overall, we do not see a strong dependence on PEO chain topology. The number of water molecules involved in hydrogen bonding (per ether oxygen) in bulk water is greater than 0.83, which is in excellent agreement with recent molecular dynamics simulation results from 36-mer linear PEO in bulk water.⁵¹ Furthermore, more than 50% of water molecules involved in hydrogen bonding are involved in multiple hydrogen bonds with PEO (from the last two columns of the table). As a result, the total number of hydrogen bonds per ether oxygen is more than 1.45, which is in very good agreement with previous simulation results. 47,51 Surprisingly, the number of hydrogen bonds drops by only 10-15% at the water/toluene interface, with the largest drop in hydrogen bond numbers coming from singly bonded water molecules. This implies that PEO chains at the water/toluene interface greatly prefer solvation by water, which is in line with the hypothesis we made earlier based on the similarities in the populations of dihedral angles of the PEO chains in water and at the water/toluene interface.

The atom—atom pair distribution functions between the PEO oxygen or carbon atoms and the toluene carbon atoms are shown in Figure 8. There is a depletion of toluene carbon atoms around the PEO oxygen atoms at the water/toluene interface compared to PEO in bulk toluene. At the same time, there is little or no depletion of the toluene carbon atoms around the PEO carbon atoms at the water/toluene interface (vs bulk toluene), indicating that the oxygen atoms of the PEO at the water/toluene interface are solvated primarily by water molecules. It is important to note that there is no difference in the pair distribution function between PEO oxygen atoms and water oxygen atoms at the water/toluene interface and in bulk water (not shown). What, then, does this suggest about the dynamics of the hydrogen bonds?

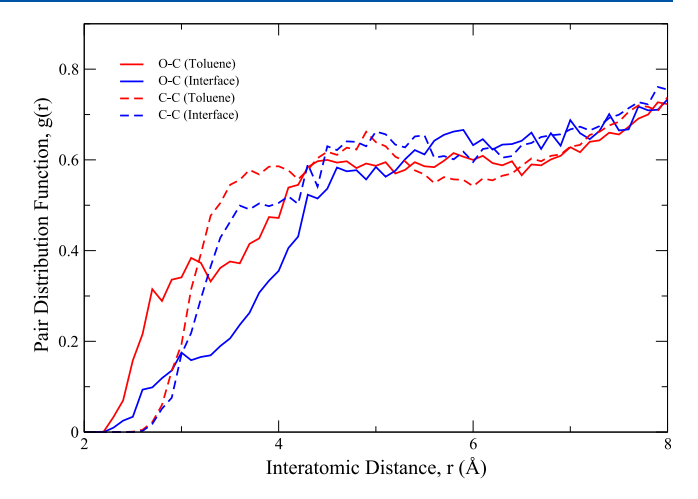


Figure 8. Pair distribution functions as a function of distance between PEO oxygens and toluene carbons (solid lines) and between PEO carbons and toluene carbons (dashed lines): in toluene (red lines) and at the water—toluene interface (blue lines).

The dynamic behavior of hydrogen bonds can be studied in terms of a history-independent (or intermittent) autocorrelation function, given by $C(t) = (\langle h(t_0)h(t_0+t) \rangle)/(\langle h(t_0)^2 \rangle)$, where h=1 if a water molecule is hydrogen bonded to PEO at a given time and 0 otherwise; thus, bonds are allowed to break and re-form. The angular brackets represent a time average over all pairs and time origins. The results of the hydrogen bond autocorrelation function are presented in Figure 9. Different approaches have been adapted in determining the average hydrogen-bond lifetime from C(t): one involves fitting the hydrogen-bond autocorrelation data to a stretched-exponential function, for the using the following Kohlrausch—Williams—Watts (KWW) stretched-exponential function:

$$C(t) = A_0 \exp[(-t/\tau)^{\beta}] \tag{5}$$

where τ is a characteristic relaxation time and the parameter β is a measure of the deviation from exponential behavior.

The average relaxation time $\langle \tau \rangle$ is then approximated by

$$\langle \tau \rangle \simeq \int_0^\infty C(t) dt = \frac{A_0 \tau}{\beta} \Gamma\left(\frac{1}{\beta}\right)$$
 (6)

where $\Gamma(x)$ is the gamma function. The fitting parameters and the average relaxation time $\langle \tau \rangle$ are listed in Table 3. The average hydrogen-bond relaxation time, $\langle \tau \rangle$, shows a strong dependence on chain topology in both bulk water and at the water/toluene interface. In bulk water, $\langle \tau \rangle$ for the ring and [2] catenane are about 27 and 47% longer, respectively, than

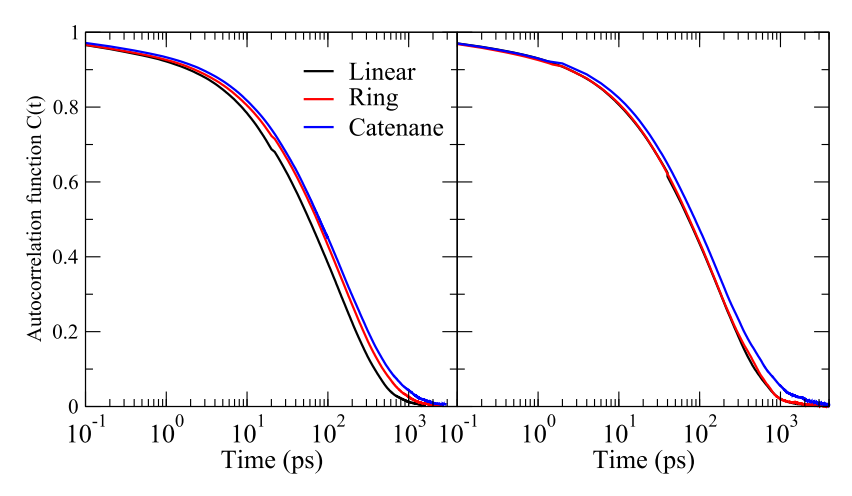


Figure 9. Hydrogen-bond autocorrelation function (normalized) for hydrogen bonds between water and linear PEO (black lines) or ring PEO (red lines) or [2] catenane (blue) in bulk water (left) and at the water/toluene interface (right).

Table 3. Fitting Parameters for the Autocorrelation Function C(t) Using Eq 5 (A_0, τ, β) and Eq 6 $(A_1, \tau_1, A_2, \tau_2, A_3, \tau_3)$

	topology	A_0	τ (ps)	β	$\langle \tau \rangle$ (ps)	A_1	τ_1 (ps)	A_2	τ_2 (ps)	A_3	τ_3 (ps)
H_2O	linear	0.96	110.9	0.66	143.0	0.08	0.72	0.32	26.2	0.60	210.6
	ring	0.96	138.7	0.65	182.0	0.11	1.85	0.35	48.9	0.54	286.4
	[2]catenane	0.98	148.9	0.62	210.6	0.11	2.26	0.35	49.7	0.54	326.7
H_2O/Tol	linear	0.97	140.5	0.65	186.2	0.10	1.43	0.30	37.0	0.60	266.4
	ring	0.97	150.2	0.64	202.5	0.11	1.12	0.36	53.5	0.53	318.8
	[2]catenane	0.98	168.3	0.61	242.9	0.12	1.41	0.41	71.1	0.47	423.1

 $\langle\tau\rangle$ for linear case. At the water/toluene interface, $\langle\tau\rangle$ for the ring and [2]catenane are about 9 and 31% longer, respectively, than they are in the linear case. Furthermore, the $\langle\tau\rangle$ for the linear, ring, and [2]catenane at the water/toluene interface are approximately 30, 11, and 15% longer, respectively, than the corresponding $\langle\tau\rangle$ in bulk water. $\langle\tau\rangle$ for the [2]catenane should be interpreted as an average value for the two rings. Thus, in both bulk water and at the water/toluene interface, catenation has a significant effect on the relaxation time of hydrogen bonds around the rings compared to an isolated ring.

The $\langle \tau \rangle$ determined using eq 5 represents an average of several hydrogen-bond relaxation times. Another approach is to separate the short- and long-term relaxation times using a linear combination of exponential functions:⁵¹

$$C(t) = A_1 \exp(-t/\tau_1) + A_2 \exp(-t/\tau_2) + A_3 \exp(-t/\tau_3)$$
(7)

where $A_3 = 1 - A_1 - A_2$, and τ_i (i = 1, 2, and 3) are relaxation times. The fitting parameters using eq 7 are also listed in Table 3. τ_1 represents the A_1 fraction of short-lived hydrogen bonds, τ_2 represents the A_2 fraction of intermediate-lived hydrogen bonds, and τ_3 represents the A_3 fraction of long-lived hydrogen bonds. From Table 3, the majority of the hydrogen bonds in all cases are long-lived and are strongly dependent on chain topology, as was the average relaxation time discussed above. About 90% of the hydrogen bonds are intermediate- and long-lived hydrogen bonds, where the long-lived are dominant. The small fraction of short-lived hydrogen bonds observed in all cases represent water molecules that are weakly hydrogen bonded to PEO oxygens. The dominant intermediate- and long-lived hydrogen bonds between PEO and water molecules in bulk water have also been observed recently. Si

Interaction Energy at the Interface. We can gain deeper insights into the interactions between water and the PEO

chains at the water/toluene interface by computing the energy of the interactions between PEO and the surrounding solvents and resolving those energies into their Coulomb and van der Waals components.

Table 4 shows the tabulated Coulomb and van der Waals (VDW) interaction energies per monomer between a PEO chain and water and/or toluene for the different topologies. The interaction energies between PEO atoms (PEO/PEO) are also reported and are stronger in water and at the water/ toluene interface due to steric hindrance within the helical structure, resulting in oxygen atoms being very close to one another, within their van der Waals radii (see Figure 4). Regardless of topology, the contribution to total interaction energy from electrostatic (Coulomb) interactions dominates the PEO-water interactions, whether in bulk water or at the water/toluene interface. The total PEO-water interaction energy at the water/toluene interface is about 80% of the total PEO-water interaction energy in bulk water, while the total PEO-toluene interaction energy at the water/toluene interface is only about 50% of the total PEO-toluene interaction energy in bulk toluene. This reinforces our earlier hypothesis that PEO chains at the water/toluene interface prefer to be solvated by water.

From Table 4, the per-monomer difference in the PEO-system interaction energy between a PEO chain in bulk water and at the water/toluene interface is on the order of $-1.2 \, \mathrm{kcal/mol}$, i.e., $2 \, k_{\mathrm{B}} T$ per monomer, realized as potentially hundreds of $k_{\mathrm{B}} T$ per chain. The sign of that difference in energy means that the energy of a PEO chain at the water/toluene interface *increases* as opposed to bulk water and implies that adsorption at the water/toluene interface is potentially drastically unfavorable, from an enthalpic standpoint of the PEO chain. Given that polymer chains exhibit decreased entropy by being confined at the interface, the entropic component of the free

Table 4. Per-Monomer Interaction Energy (kcal/mol/Monomer) of a PEO Chain at the Water/Toluene Interface, Broken down by Interactions with Itself (PEO/PEO) and with Each Solvent (PEO/H,O, PEO/Toluene), Each Further Broken down into Coulomb and Van Der Waals Contributions Alongside the Total; the Per-Monomer Total Interaction Energy Is Also Displayed

			PEO/PEO				PEO/H_2O			PEO/system
topology	ဘိ	Coulomb	Mpa	total		Coulomb	Mpa	total		total
linear	5.59	5.59 ± 0.17	0.36 ± 0.10	5.95 ± 0.20		-15.40 ± 0.60	-3.32 ± 0.19	-18.71 ± 0.58	·	-12.71 ± 0.58
ring	5.60	5.60 ± 0.17	0.31 ± 0.12	5.90 ± 0.22		-15.34 ± 0.61	-3.24 ± 0.21	-18.58 ± 0.61		-12.68 ± 0.48
[2]catenane	5.53	5.53 ± 0.08	0.25 ± 0.09	5.78 ± 0.15		-15.17 ± 0.42	-3.19 ± 0.14	-18.36 ± 0.41		-12.58 ± 0.34
			PEO/PEO				PEO/toluene			PEO/system
topology	ŭ	Coulomb	Mpa	total		Coulomb	Mpa	total	al l	total
linear	3.00	3.00 ± 0.17	-0.44 ± 0.25	2.63 ± 0.37		-0.81 ± 0.12	-4.38 ± 0.40	-5.20 ± 0.50	5 0.50	-2.64 ± 0.25
ring	3.02	3.02 ± 0.16	-0.39 ± 0.24	2.63 ± 0.36		-0.83 ± 0.12	-4.44 ± 0.39	-5.27 ± 0.48	5 0.48	-2.64 ± 0.25
[2]catenane	2.82	2.82 ± 0.10	-0.90 ± 0.16	1.92 ± 0.23		-0.67 ± 0.08	-3.63 ± 0.24	-4.30 ± 0.30	: 0.30	-2.38 ± 0.17
		PEO/PEO			PEO/H_2O			PEO/toluene		PEO/system
topology	Coulomb	Mpa	total	Coulomb	Mpa	total	Coulomb	Mpa	total	total
linear	5.36 ± 0.17	0.43 ± 0.09	5.80 ± 0.23	-12.80 ± 0.22	-1.80 ± 0.22	-14.72 ± 0.81	-0.40 ± 0.09	-2.17 ± 0.24	-2.57 ± 0.27	-11.50 ± 0.51
ring	5.38 ± 0.16	0.41 ± 0.09	5.79 ± 0.19	-12.91 ± 0.71	-1.82 ± 0.21	-14.73 ± 0.78	-0.39 ± 0.09	-2.11 ± 0.24	-2.51 ± 0.30	-11.45 ± 0.53
[2]catenane	5.31 ± 0.12	0.31 ± 0.08	5.58 ± 0.15	-12.95 ± 0.52	-1.94 ± 0.17	-14.80 ± 0.57	-0.33 ± 0.06	-1.80 ± 0.18	-2.13 ± 0.24	-11.40 ± 0.39

energy also does not favor PEO adsorption at the water/ toluene interface. Furthermore, based on these findings, we expect a PEO chain at the water/toluene interface to be surrounded mostly by water molecules that are strongly bound to PEO oxygen atoms through hydrogen bonding. As a result, the water molecules around a PEO chain are already in a state of low translational and rotational entropy and thus should not favor the absorption of the PEO chain at the interface. This poses the question: what is the driving force for a PEO chain to adsorb at the water/toluene interface? To answer this, we also computed the total interaction energy between the water and toluene molecules in the presence and absence of a PEO chain at the interface. In the presence of a PEO chain at the interface, we found a decrease in the total enthalpic interaction energy between water and toluene molecules of about 2.6 kcal/mol per monomer, i.e., more than two times the above-reported increase in the enthalpic interaction of the PEO chain caused by adsorption at the interface. Thus, a PEO chain can be thought of as adsorbing at the water/toluene interface in order to "screen" the water molecules from the toluene molecules, reducing the unfavorable interfacial interaction between water and toluene molecules (this is in agreement with earlier simulation using a bead-spring model⁷).

CONCLUSION

In the preceding work, we have sought to understand the differences caused by variations in polymer topology on the solvation structure and energetics of linear, ring, and [2]catenane PEO chains in water, in toluene, and at a water/toluene interface. Our initial observations suggested that even when confined to an interface between immiscible solvents, all three chain topologies prefer to extend toward the aqueous side of the interface rather than the toluene side, marking water as a clearly better solvent, regardless of polymer topology or overall size. However, all three proposed measures of overall polymer "shape"—radius of gyration and the derived asphericity and prolateness-agree to the pronounced tendency of each topology to spread out along the water/ toluene interface. Among the three topologies, linear PEO showed the largest increase in R_g at the water/toluene interface compared to its R_g in water or toluene.

The total number of hydrogen bonds between PEO oxygens and water molecules is reduced by only 10-15% at the interface compared in bulk water, and the hydrogen bonds formed between PEO and water at the interface are considerably longer-lived and strongly dependent on chain topology, suggesting a significant strengthening of PEO-water interactions when the water/toluene interface is present. However, analysis of the interaction energies between PEO and molecules of the solvents in an interfacial environment suggests both an entropic penalty and an enthalpic penalty of about 1.2 kcal/mol/monomer when any of the PEO chains are at the water/toluene interface. This led us to consider what kind of interactions dominate the energetics of adsorption of each polymer topology at the interface, and interestingly, it appears the driving force for chains to spread out along the interface is primarily due to a need to "screen" solvent molecules from one another across the interface, rather than any energetic or enthalpic favorability between the PEO chains and the solvents themselves. This has stimulated us to consider future simulation efforts involving generalizable solvent-chain interactions with bead-spring models to investigate the

interplay between solvent quality, polymer topology, and interfacial adsorption.

AUTHOR INFORMATION

Corresponding Author

Mesfin Tsige — School of Polymer Science and Polymer Engineering, The University of Akron, Akron, Ohio 44325, United States; ⊙ orcid.org/0000-0002-7540-2050; Phone: 330-972-5631; Email: mtsige@uakron.edu; Fax: 330-972-5290

Authors

Saeed Akbari Shandiz — Department of Macromolecular Science & Engineering, Case Western Reserve University, Cleveland, Ohio 44106, United States; orcid.org/0000-0002-4232-8069

Gary M. Leuty – LinQuest Corporation, Beavercreek, Ohio 45431, United States

Hao Guo − School of Polymer Science and Polymer Engineering, The University of Akron, Akron, Ohio 44325, United States; orcid.org/0000-0002-5649-6346

Abdol Hadi Mokarizadeh – School of Polymer Science and Polymer Engineering, The University of Akron, Akron, Ohio 44325, United States; orcid.org/0000-0001-5922-7654

Joao M. Maia – Department of Macromolecular Science & Engineering, Case Western Reserve University, Cleveland, Ohio 44106, United States

Complete contact information is available at: https://pubs.acs.org/10.1021/acs.langmuir.3c00589

Author Contributions

S.A.S. and G.M.L. contributed equally to this work.

Notes

The authors declare no competing financial interest.

ACKNOWLEDGMENTS

H.G., A.H.M., and M.T. acknowledge financial support from the National Science Foundation (DMR-1912329 and DMR-2114640).

REFERENCES

- (1) Davidson, M. L.; Laufer, L.; Gottlieb, M.; Walker, L. M. of Flexible, Oil-Soluble Diblock and BAB Triblock Copolymers to Oil/Water Interfaces. *Langmuir* **2020**, *36*, 7227–7235.
- (2) Qin, B.; Xu, J.; Zhang, X. Supramolecular Polymerization at Interfaces. *Langmuir* **2022**, *38*, 4157–4163.
- (3) Luz, A. M.; Barbosa, G.; Manske, C.; Tavares, F. W. Tween-80 on Water/Oil Interface: Structure and Interfacial Tension by Molecular Dynamics Simulations. *Langmuir* **2023**, *39*, 3255–3265.
- (4) Costa, L.; Li-Destri, G.; Thomson, N. H.; Konovalov, O.; Pontoni, D. Real Space Imaging of Nanoparticle Assembly at Liquid-Liquid Interfaces with Nanoscale Resolution. *Nano Lett.* **2016**, *16*, 5463–5468.
- (5) Raphael, E.; Pincus, P.; Fredrickson, G. H. Conformation of Star Polymers in High Molecular Weight Solvents. *Macromolecules* **1993**, 26, 1996–2006.
- (6) Huissmann, S.; Blaak, R.; Likos, C. N. Star Polymers in Solvents of Varying Quality. *Macromolecules* **2009**, 42, 2806–2816.
- (7) Taddese, T.; Carbone, P.; Cheung, D. L. Thermodynamics of Linear and Star Polymers at Fluid Interfaces. *Soft Matter* **2015**, *11*, 81–93.
- (8) Hegde, G. A.; Chang, J.-f.; Chen, Y.-l.; Khare, R. Conformation and Diffusion Behavior of Ring Polymers in Solution: A Comparison

- Between Molecular Dynamics, Multiparticle Collision Dynamics, and Lattice Boltzmann Simulations. J. Chem. Phys. 2011, 135, 184901.
- (9) Damjanovic, J.; Miao, J.; Huang, H.; Lin, Y.-S. Elucidating Solution Structures of Cyclic Peptides Using Molecular Dynamics Simulations. *Chem. Rev.* **2021**, *121*, 2292–2324.
- (10) Huber, H. F.; Thies, C. Adsorption of Toluene-Soluble Polymers at the Toluene-Water Interface. *J. Polym. Sci.: Part A-2* 1970, 8, 71–80.
- (11) Prokop, R. M.; Hair, M. L.; Neumann, A. W. Interfacial Tension of a Polystyrene-Poly(ethylene oxide) Diblock Copolymer at teh Water-Toluene Interface. *Macromolecules* **1996**, *29*, 5902–5906.
- (12) Taddese, T.; Cheung, D. L.; Carbone, P. Scaling Behavior of Polymers at Liquid/Liquid Interfaces. ACS. Macro. Lett. 2015, 4, 1089–1093.
- (13) Giunta, G.; Carbone, P. Cross-over in the Dynamics of Polymer Confined Between Two Liquids of Different Viscosity. *Interface Focus* **2019**, *9*, 20180074.
- (14) Stoddart, J. F. Mechanically Interlocked Molecules (MIMs) Molecular Shuttles, Switches, and Machines (Nobel Lecture). *Angew. Chem., Int. Ed.* **2017**, *56*, 11094—11125.
- (15) Vologodskii, A. V.; Cozzarelli, N. R. Monte Carlo Analysis of the Conformation of DNA Catenanes. *J. Mol. Biol.* **1993**, 232, 1130–1140
- (16) Laurie, B.; Katritch, V.; Sogo, J.; Koller, T.; Dubochet, J.; Stasiak, A. Geometry and Physics of Catenanes Applied to the Study of DNA Replication. *Biophys. J.* **1998**, 74, 2815–2822.
- (17) Hudson, B.; Vinograd, J. Catenated Circular DNA Molecules in HeLa Cell Mitochondria. *Nature* **1967**, *216*, 647–652.
- (18) Vologodskii, A.; Rybenkov, V. V. Simulation of DNA Catenanes. *Phys. Chem. Chem. Phys.* **2009**, *11*, 10543–10552.
- (19) Schmidt, T. L.; Heckel, A. Construction of a Structurally Defined Double-Stranded DNA Catenane. *Nano Lett.* **2011**, *11*, 1739–1742.
- (20) Stulz, E. DNA Architectonics: Towards the Next Generation of Bio-Inspired Materials. *Chem.—Eur. J.* **2012**, *18*, 4456–4469.
- (21) Lu, C.-H.; Cecconello, A.; Elbaz, J.; Credi, A.; Willner, I. A Three-Station DNA Catenane Rotary Motor with Controlled Directionality. *Nano Lett.* **2013**, *13*, 2303–2308.
- (22) Elbaz, J.; Cecconello, A.; Fan, Z.; Govorov, A. O.; Willner, I. Powering the Programmed Nanostructure and Function of Gold Nanoparticles with Catenated DNA Machines. *Nature Comm.* **2013**, *4*, 2000.
- (23) Wikoff, W. R.; Liljas, L.; Duda, R. L.; Tsuruta, H.; Hendrix, R. W.; Johnson, J. E. Topologically Linked Protein Rings in the Bacteriophage HK97 Capsid. *Science* **2000**, 289, 2129–2133.
- (24) Helgstrand, C.; Wikoff, W. R; Duda, R. L; Hendrix, R. W; Johnson, J. E; Liljas, L. The Refined Structure of a Protein Catenane: The HK97 Bacteriophage Capsid at 3.44 Å Resolution. *J. Mol. Biol.* **2003**, 334, 885–899.
- (25) White, H. E.; Sherman, M. B.; Brasilès, S.; Jacquet, E.; Seavers, P.; Tavares, P.; Orlova, E. V. Capsid Structure and Its Stability at the Late Stages of Bateriophage SPP1 Assembly. *J. Virol.* **2012**, *86*, 6768–6777.
- (26) Shimada, S.; Ishikawa, K.; Tamaoki, N.; et al. Synthesis and Switchable Condensation Reaction of Bifunctional [2] Catenane. *Acta Chem. Scand.* **1998**, 52, 374–376.
- (27) Hamers, C.; Raymo, F. M.; Stoddart, J. F. Main-Chain and Pendant Poly([2]catenane)s Incorporating Complementary π -Electron-Rich and -Deficient Components. *Eur. J. Org. Chem.* **1998**, 1998, 2109–2117.
- (28) Raehm, L.; Kern, J.-M.; Sauvage, J.-P.; Hamann, C.; Palacin, S.; Bourgoin, J.-P. *Eur. J.* **2002**, *8*, 2153–2162.
- (29) Wasserman, E. The Preparation of Interlocking Rings: A Catenane. J. Am. Chem. Soc. 1960, 82, 4433-4434.
- (30) Schill, G.; Lüttringhaus, A. The Preparation of Catena Compounds by Directed Synthesis. *Angew. Chem., Int. Ed. Engl.* **1964**, *3*, 546–547.

- (31) Dietrich-Buchecker, C. O.; Sauvage, J. P. Synthese de composes polyethers macrocycliques derives de la phenanthroline-1,10 diphenyl-2,9. *Tetrahedron Lett.* **1983**, *24*, 5091–5094.
- (32) Anelli, P. L.; et al. Molecular meccano. 1. [2]Rotaxanes and a [2]catenane made to order. J. Am. Chem. Soc. 1992, 114, 193–218.
- (33) Amabilino, D. B.; Ashton, P. R.; Reder, A. S.; Spencer, N.; Stoddart, J. F. Olympiadane. *Angew. Chem., Int. Ed. Engl.* **1994**, 33, 1286–1290.
- (34) Fang, L.; Olson, M. A.; Benitez, D.; Tkatchouk, E.; Goddard, W. A., III; Stoddart, J. F. Mechanically Bonded Macromolecules. *Chem. Soc. Rev.* **2010**, *39*, 17–29.
- (35) Griffiths, K. E.; Stoddart, J. F. Template-Directed Synthesis of Donor/Acceptor [2] Catenanes and [2] Rotaxanes. *Pure Appl. Chem.* **2008**, *80*, 485–506.
- (36) Wu, Q.; Rauscher, P. M.; Lang, X.; Wojtecki, R. J.; de Pablo, J. J.; Hore, M. J. A.; Rowan, S. J. Poly[n]catenanes: Synthesis of Molecular Interlocked Chains. *Science* **2017**, 358, 1434–1439.
- (37) Rane, S. S.; Mattice, W. L. Structure and Internal Dynamics of Poly(ethylene oxide) Catenanes in the Melt. *Macromolecules* **2005**, *38*, 3708–3712.
- (38) Pakula, T.; Jeszka, K. Simulation of Single Complex Macromolecules. 1. Structure and Dynamics of Catenanes. *Macromolecules* 1999, 32, 6821–6830.
- (39) Rauscher, P. M.; Rowan, S. J.; de Pablo, J. J. Topological Effects in Isolated Poly[n]catenanes: Molecular Dynamics Simulations and Rouse Mode Analysis. *ACS Macro Lett.* **2018**, *7*, 938–943.
- (40) Rauscher, P. M.; Schweizer, K. S.; Rowan, S. J.; de Pablo, J. J. Thermodynamics and Structure of Poly[n]catenane Melts. *Macromolecules* **2020**, *53*, 3390–3408.
- (41) Rauscher, P. M.; Schweizer, K. S.; Rowan, S. J.; de Pablo, J. J. Dynamics of Poly[n]catenane Melts. *J. Chem. Phys.* **2020**, *152*, 214901.
- (42) Chmielewski, M. J.; Davis, J. J.; Beer, P. D. Interlocked Host Rotaxane and Catenane Structures for Sensing Charged Guest Species via Optical and Electrochemical Methodologies. *Org. Biomol. Chem.* **2009**, *7*, 415–424.
- (43) Suzuki, J.; Takano, A.; Matsushita, Y. Dimensions of Catenated Ring Polymers in Dilute Solution Studied by Monte-Carlo Simulation. *J. Chem. Phys.* **2018**, *149*, 204901.
- (44) Bauer, B. J.; Hadjichristidis, N.; Fetters, L. J.; Roovers, J. E. L. Star-Branched Polymers. 5. The Θ Temperature Depression for 8-and 12-Arm Polyisoprenes in Dioxane. *J. Am. Chem. Soc.* **1980**, *102*, 2410–2413.
- (45) Iwata, K. Θ Temperature of Ring Polymers: Another Evidence of Topological Interaction. *Macromolecules* **1989**, *22*, 3702–3706.
- (46) Suzuki, J.; Takano, A.; Matsushita, Y. The theta-temperature Depression Caused by Topological Effect in Ring Polymers Studied by Monte Carlo Simulation. *J. Chem. Phys.* **2011**, *135*, 204903.
- (47) Smith, G. D.; Bedrov, D.; Borodin, O. Molecular Dynamics Simulation Study of Hydrogen Bonding in Aqueous Poly(ethylene oxide) Solutions. *Phys. Rev. Lett.* **2000**, *85*, 5583–5586.
- (48) Dormidontova, E. E. Role of Competitive PEO-Water and Water-Water Hydrogen Bonding in Aqueous Solution PEO Behavior. *Macromolecules* **2002**, *35*, 987–1001.
- (49) Lee, H.; de Vries, A. H.; Marrink, S.-J.; Pastor, R. W. A Coarse-Grained Model for Polyethylene Oxide and Polyethylene Glycol: Conformation and Hydrodynamics. *J. Phys. Chem. B* **2009**, *113*, 13186–13194.
- (50) Hezaveh, S.; Samanta, S.; Milano, G.; Roccatano, D. Molecular Dynamics Simulation Study of Solvent Effects on Conformation and Dynamics of Polyethylene Oxide and Polypropylene Oxide Chains in Water and in Common Organic Solvents. *J. Chem. Phys.* **2012**, *136*, 124901.
- (51) Dahal, U. R.; Dormidontova, E. E. The Dynamics of Solvation Dictates the Conformation of Polyethylene oxide in Aqueous, isobutyric acid and Binary Solutions. *Phys. Chem. Chem. Phys.* **2017**, 19, 9823–9832.
- (52) Sherck, N.; Webber, T.; Brown, D. R.; Keller, T.; Barry, M.; DeStefano, A.; Jiao, S.; Segalman, R. A.; Fredrickson, G. H.; Shell, M.

- S.; Han, S. End-to-End Distance Probability Distributions of Dilute Poly(ethylene oxide) in Aqueous Solution. *J. Am. Chem. Soc.* **2020**, 142, 19631–19641.
- (53) Couper, A.; Stepto, R. F. T. Diffusion of low-molecular weight poly(ethylene oxide) in water. *Trans. Faraday Soc.* **1969**, *65*, 2486–2496.
- (54) Kjellander, R.; Florin, E. Water Structure and Changes in Thermal Stability of the System Poly (ethylene oxide)-Water. *J. Chem. Soc., Faraday Trans.* **1981**, *77*, 2053–2077.
- (55) Kawaguchi, S.; Imai, G.; Suzuki, J.; Miyahara, A.; Kitano, T.; Ito, K. Aqueous Solution Properties of Oligo- and Poly(ethylene oxide) by Static Light Scattering and Intrinsic Viscosity. *Polymer* 1997, 38, 2885–2891.
- (56) Shephard, J. J.; Bremer, P. J.; McQuillan, A. J. Structure and Conformation in Mixtures of Methyl-Terminated Poly(ethylene oxide) and Water. Principal Component Analysis and Band Fitting of Infrared Absorptions. J. Phys. Chem. B 2009, 113, 14229–14238.
- (57) Grinberg, V. Y.; Burova, T. V.; Grinberg, N. V.; Dubovik, A. S.; Papkov, V. S.; Khokhlov, A. R. Energetics of LCST Transition of Poly(ethylene oxide) in Aqueous Solutions. *Polymer* **2015**, *73*, 86–90.
- (58) Teleszewski, T.; Gajewski, A. Measurement Approach of Interfacial Tension on Example of Water-Toluene. *Int. Commun. Heat Mass* **2020**, *118*, 104817.
- (59) Hanwell, M. D.; Curtis, D. E.; Lonie, D. C.; Vandermeersch, T.; Zurek, E.; Hutchison, G. R. AAvogadro: An Advanced Semantic Chemical Editor, Visualization and Analysis Platform. *J. Cheminformatics* **2012**, *4*, 17.
- (60) Jorgensen, W. L.; Maxwell, D. S.; Tirado-Rives, J. Development and Testing of the OPLS All-Atom Force Field on Conformational Energetics and Properties of Organic Liquids. *J. Am. Chem. Soc.* **1996**, 118, 11225–11236.
- (61) Thompson, A. P.; Metin, H. LAMMPS A Flexible Simulation Tool for Particle-Based Materials Modeling at the Atomic, Meso, and Continuum Scales. *Comput. Phys. Commun.* **2022**, *271*, 108171.
- (62) Marques, C.; Joanny, J. F.; Leibler, L. Adsorption of Block Copolymers in Selective Solvents. *Macromolecules* **1988**, *21*, 1051–1059.
- (63) Cai, S.; Liu, J.; Tian, M.; Wang, K.; Shen, L. Diffusion Dynamics of a Single Collapsed Homopolymer Globule at the Solid-Liquid Interface. *Soft Matter* **2020**, *16*, 2431–2436.
- (64) Glen, N. F.; Johns, A. I. Determination of the Density of Toluene in the Range from (293 to 373) K and from (0.1 to 30) MPa. *J. Chem. Eng. Data* **2009**, 54, 2538–2545.
- (65) Tasaki, K.; Abe, A. NMR Studies and Conformational Energy Calculations of 1,2-Dimethoxyethane and Poly(oxyethylene). *Polym. J.* 1985, 17, 641.
- (66) Tasaki, K. Poly(oxyethylene)-Water Interactions: A Molecular Dynamics Study. J. Am. Chem. Soc. 1996, 118, 8459–8469.
- (67) Bedrov, D.; Smith, G. The role of local conformations in the stretching of a poly(ethylene oxide) chain in solution. *J. Chem. Phys.* **2003**, *118*, 6656.
- (68) Lee, H.; Venable, R. M.; MacKerell, A. D.; Pastor, R. W. Molecular Dynamics Studies of Polyethylene Oxide and Polyethylene Glycol: Hydrodynamic Radius and Shape Anisotropy. *Biophsical Journal* **2008**, *95*, 1590–1599.
- (69) Tsige, M.; Mahajan, M. P.; Rosenblatt, C.; Taylor, P. L. Nematic Order in Nanoscopic Liquid Crystal Droplets. *Phys. Rev. E* **1999**, *60*, 638–644.
- (70) Gartner, T. E. I.; Haque, F. M.; Gomi, A. M.; Grayson, S. M.; Hore, M. A. J.; Jayaraman, A. Scaling Exponent and Effective Interactions in Linear and Cyclic Polymer Solutions: Theory, Simulations, and Experiments. *Macromolecules* **2019**, *52*, 4579–4589.
- (71) Takano, A.; Ohta, Y.; Masuoka, K.; Matsubara, K.; Nakano, T.; Hieno, A.; Itakura, M.; Takahashi, K.; Kinugasa, S.; Kawaguchi, D.; Takahashi, Y.; Matsushita, Y. Radii of Gyration of Ring-Shaped Polystyrenes with High Purity in Dilute Solutions. *Macromolecules* **2012**, *45*, 369–373.
- (72) Gkolfi, E.; Bačová, P.; Harmandaris, V. Size and Shape Characteristics of Polystyrene and Poly(ethylene oxide) Star Polymer

Melts Studied by Atomistic Simulations. *Macromol. Theory Simul.* **2021**, *30*, 2000067.

- (73) Bekele, S.; Tsige, M. Interfacial Properties of Oxidized Polystyrene and its Interaction with Water. *Langmuir* **2013**, 29, 13230–13238.
- (74) Bekele, S.; Tsige, M. Characterizing the Hydrophobicity of Surfaces Using the Dynamics of Interfacial Water Molecules. *J. Phys. Chem. C* **2018**, *122*, 9015–9020.

□ Recommended by ACS

Supramolecular Networks Obtained by Block Copolymer Self-Assembly in a Polymer Matrix: Crystallization Behavior and Its Effect on the Mechanical Response

Ruth N. Schmarsow, Walter F. Schroeder, et al.

FEBRUARY 07, 2023 MACROMOLECULES

READ 🗹

Simulating Assembly Landscapes for Comprehensive Understanding of Supramolecular Polymer–Solvent Systems

Stef A. H. Jansen, E. W. Meijer, et al.

FEBRUARY 09, 2023

JOURNAL OF THE AMERICAN CHEMICAL SOCIETY

READ 🗹

Effective Design for Long-Range Polymer Ordering Using Triptycene-Containing Side Chains

Jiatong Yu, Takanori Fukushima, et al.

JUNE 07, 2023 MACROMOLECULES

READ 🗹

One-Pot Synthesis of Miktoarm Star Polymers Based on Orthogonal Metal-Ligand Interactions

Thomas Bätz, Ulrich S. Schubert, et al.

JANUARY 09, 2023

ACS APPLIED POLYMER MATERIALS

READ 🗹

Get More Suggestions >